JTTEE5 18:921–933
DOI: 10.1007/s11666-009-9325-2
1059-9630/$19.00 © ASM International

Modeling Aspects of High Velocity Impact of Particles in Cold Spraying by Explicit Finite Element Analysis

Wen-Ya Li, Chao Zhang, Chang-Jiu Li, and Hanlin Liao

(Submitted January 15, 2009; in revised form March 24, 2009)

In this study, an examination of cold spray particle impacting behavior using the ABAQUS/Explicit program was conducted for typical copper material (OFHC). Various combinations of calculation settings concerning element type, Arbitrary Lagrangian Eulerian adaptive meshing, contact interaction, material damage, etc., were examined with the main focus on the element excessive distortion and its effect on the resultant output. The effect of meshing size on the impact behavior was also clarified compared to the previous results obtained by using the LS-DYNA code. Some fundamental aspects on modeling of cold spray particle deformation are discussed.

Keywords cold spraying, copper particles, deformation behavior, explicit finite element analysis, high velocity impact

1. Introduction

Cold spraying is a coating technology on the basis of aerodynamics and high-speed impact dynamics. In this process, spray particles (usually 5-50 μm in diameter) are accelerated to a high velocity (typically 300-1200 m/s) by a high-speed gas flow that is generated through a convergent-divergent de Laval type nozzle. A coating is formed through the intensive plastic deformation of particles impacting on a substrate at a temperature well below the melting point of the spray material. This phenomenon has been discovered during the test of supersonic wind tunnel in the middle of 1980s at the Institute for Theoretical and Applied Mechanics of the Siberian Division of the Russian Academy of Science in Novosibirsk and firstly reported by the Russian scientists (Ref 1). It has been widely investigated by both numerical and experimental methods owing to its advantages over the conventional thermal spray processes to deposit a wide variety of metals, alloys, and composites (Ref 2). Although it has great application potentials in aerospace, automobile manufacture, chemical industry, etc., there are still some important aspects to be well revealed including the actual bonding mechanism of spray particles.

As for the bonding mechanism of cold spray particles, the most prevailing hypothesis is that plastic deformation may disrupt thin surface films, such as oxides, and provide intimate conformal contact under high local pressure, thus permitting bonding to occur. And thus, this bonding process was considered to be comparable to that in process such as explosive welding or shock wave powder compaction (Ref 3-5). It was also reported that the formation of jetting at the local intensively deformed zones could be helpful in the cleaning of the crushed oxide films (Ref 3-8). The above-mentioned bonding hypothesis is consistent with the fact that a wide range of ductile materials, such as metals and alloys, have been deposited by cold spray and the spray particles experience extensive deformation to form lens-like shapes. Non-ductile materials, such as ceramics, can be only deposited if they are co-cold-sprayed with a ductile (matrix) material or sprayed on a ductile substrate to form a thin layer. This hypothesis can also explain the observed critical velocity necessary to achieve a successful deposition (Ref 7-9). However, there are still some fundamental problems to be revealed, such as the metal jetting and shear instability at the contact interfaces. On the other hand, the observed critical velocity was demonstrated to be influenced by the particle size (Ref 5), temperature (Ref 4-6, 9), and its oxidation state (Ref 6, 10-12) besides the mechanical properties of given particle and substrate materials (Ref 1, 2). Therefore, it is of significant importance to study the deformation behavior of cold spray particles upon impact.

A few studies focused on the impacting and deformation behaviors of spray particles by experiments or

Wen-Ya Li, Shaanxi Key Laboratory of Friction Welding Technologies, School of Materials Science and Engineering, Northwestern Polytechnical University, 127, West Youyi Road, Xi'an, Shaanxi 710072, P.R. China; **Chao Zhang**, State key Laboratory for Mechanical Behavior of Materials, School of Materials Science and Engineering, Xi'an Jiaotong University, Xi'an, Shaanxi, P.R. China and LERMPS, Université de Technologie de Belfort-Montbéliard, Site de Sévenans, Belfort Cedex, France; and **Chang-Jiu Li**, State key Laboratory for Mechanical Behavior of Materials, School of Materials Science and Engineering, Xi'an Jiaotong University, Xi'an, Shaanxi, P.R. China; and **Hanlin Liao**, LERMPS, Université de Technologie de Belfort-Montbéliard, Site de Sévenans, Belfort Cedex, France. Contact e-mail: liwy@nwpu.edu.cn.

simulations. Because of the very short duration of particle impact (tens of nanoseconds), it is very difficult to observe the whole deformation process of particles. Only the deformed particles can be observed by microscopy. Therefore, the numerical method takes an important role in studying the particle deformation process. In some studies (Ref 3, 7), a coupled thermal-mechanical/hydrodynamic (CTH) code, developed at Sandia National Laboratories (Albuquerque, NM, USA) for modeling complex multidimensional, multiproblems that are characterized by large deformation and/or strong shocks, was used. This is based on a two-step Eulerian solution algorithm. Two explicit finite element analysis (FEA) softwares, ABAQUS (Ref 4, 5, 8) and LS-DYNA (Ref 6, 9, 10) were also used to investigate the cold spray particle impacting behavior. These two explicit FEA programs are widely used to solve the engineering problems involving in nonlinear dynamic processes.

The reported numerical results in literature (Ref 3-10) have indicated that the flattening ratio of particles increases with the increase in particle impact velocity, which is comparable to the experiment results. Moreover, the temperature at localized contact interfaces rises remarkably due to the possible adiabatic shear process. Through numerical simulations by ABAQUS, Assadi et al. (Ref 4, 5) found that the instability of adiabatic shear flow occurs as particle velocity becomes higher than a critical velocity. Therefore, they took this velocity as the actual critical velocity for particle deposition in cold spray. However, owing to the excessive distortion of meshing at the local contact zones in simulation by the Lagrangian algorithm, this calculated critical velocity is much dependent on the meshing size (Ref 6, 9). In the previous study (Ref 9), when the Arbitrary Lagrangian Eulerian (ALE) method available in LS-DYNA was used to avoid the problems associated with the severe mesh distortion, no steep change of plastic strain or temperature was observed, which was used to indicate the onset of the shear instability by Assadi et al. (Ref 4, 5). Accordingly, it seems that the steep change of plastic strain obtain by the Lagrangian method is attributed to the abnormal deformation of elements and cannot be directly associated with the actual shear instability upon particle impacting. In addition, Schmidt et al. (Ref 5) also found the dependence of critical velocity on particle size by simulations using ABAQUS with the Lagrangian algorithm. Although the experiments have shown the effect of particle size on critical velocity (Ref 5), their simulation results obtained by the Lagrangian algorithm are believed to be unreasonable. The recent studies have shown the effect of oxide films on particle critical velocity (Ref 6, 10, 12). Considering the fact that the small powders normally have higher oxygen contents than those of large powders (Ref 13), it is expected that the oxide films on particles surfaces is the main factor influencing critical velocity besides the material mechanical properties. Schmidt et al. (Ref 5) also explained the possible reasons causing the effect of particle size. They thought that high cooling rates, high strain rates, high viscous shear strength, and high surface contaminations such as oxide shells of small particles possibly hinder the particle deformation and thus increase the critical velocity (Ref 5). However, these views need further experimental study to be clarified.

In this study, numerical simulation of cold spray particle impacting behavior using the ABAQUS program was conducted for typical copper material (OFHC). Various combinations of calculation settings concerning element type, ALE adaptive meshing, contact interaction, material damage, etc., were examined with the main focus on the element excessive distortion and its effect on the resultant output. The effects of meshing size and particle size on the impact behavior were also clarified compared to the previous results obtained using the LS-DYNA code.

2. Numerical Method

The impacting behavior of a particle on a substrate was modeled using an explicit FEA program ABAQUS/Explicit with the Lagrangian formulation (Ref 14). Owing to the axisymmetric characteristic of normal impact process, a 2D symmetric model was used as shown in Fig. 1. In this study, the substrate was taken as a cylinder. The radius and height of the substrate were taken to be five times larger than the particle diameter (e.g., 20 μm). For the convenience of meshing, the computational domain was partitioned into several regions as shown in Fig. 1(a). The meshing was conducted by using the 4-node quad element with coupled displacement and temperature, reduced integration and hourglass control as shown in Fig. 1(b). The nominal meshing size for the particle was 0.4 μm (a meshing resolution of $1/50d_p$) for a 20-μm particle. The interface region in the substrate has the element size of 1.2 times of that of particle (0.48 μm in case of a 20-μm particle) in order to avoid the large deformation of substrate surface elements. Different meshing sizes were examined in this study. Based on the previous simulation results (Ref 4-6, 8, 9), the elements at the particle surface were monitored and used for the output of results, which experience almost the maximum plastic strain during impacting. In the previous studies (Ref 4, 8), the impacting process was assumed to be an adiabatic process; i.e., the heat transfer is not considered based on a simple estimation. However, a recent study by Schmidt et al. (Ref 5) and our preliminary simulations indicated that the heat conduction should be considered in most cases. Therefore, in this study, both the Dynamic-Explicit procedure including adiabatic heating effects and the Dynamic-Temperature-Displacement-Explicit procedure available in ABAQUS were used to clarify this effect.

The particle/substrate interaction was implemented by using the surface-to-surface contact (Explicit) formulation available in ABAQUS. In this study, the friction between the particle and substrate was also considered with different coefficients of friction (COFs). The temperature rise is based on the commonly used empirical assumption that 90% of plastic work and 100% friction work is dissipated as heat.

For particles and substrates, the material deformation was described by the Johnson and Cook (JC) plasticity

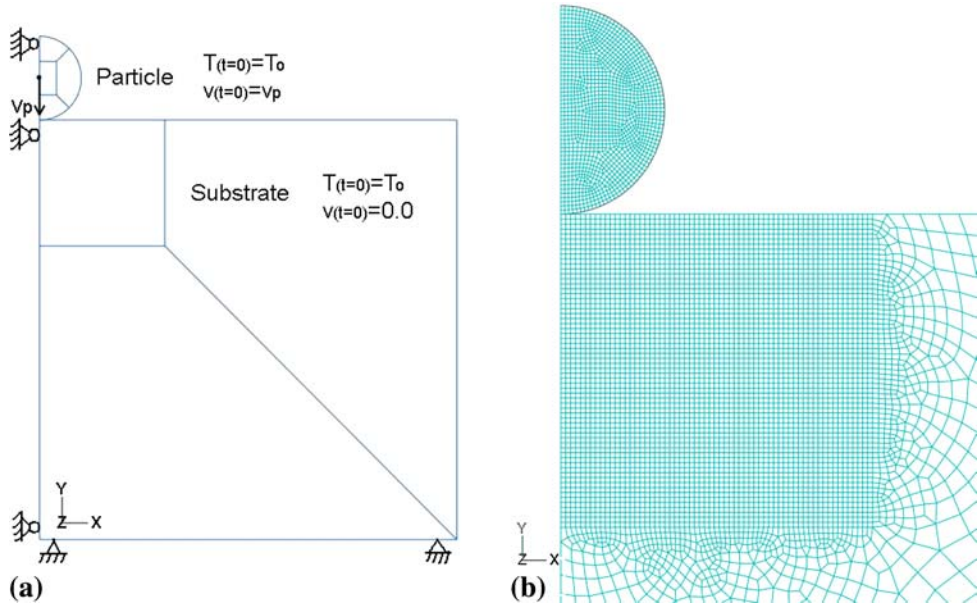

Fig. 1 (a) Computational domain and the initial and boundary conditions; (b) meshing arrangement (meshing resolution of $1/50d_p$ for a 20 μm particle)

model, which accounts for strain hardening, strain rate hardening, and thermal softening effects. The stresses were expressed according to the Von Mises plasticity model. The flow stress (σ) of material is expressed as follows (Ref 14, 15):

$$\sigma = (A + B\varepsilon_p^n)(1 + C\ln(\dot{\varepsilon}^*))(1 - (T^*)^m) \quad \text{(Eq 1)}$$

where A, B, n, C, m are the constants dependent on materials. ε_p is the effective plastic strain (PEEQ). $\dot{\varepsilon}^*$ is the effective plastic strain rate normalized with respect to a reference strain rate ($\dot{\varepsilon}_p/\dot{\varepsilon}_o$). T^* is a homologous temperature defined as the following (Ref 14, 15).

$$T^* = \begin{cases} 0 & \text{for } T < T_r \\ (T - T_r)/(T_m - T_r) & \text{for } T_r \le T \le T_m \\ 1 & \text{for } T > T_m \end{cases} \quad \text{(Eq 2)}$$

where T_m is the melting temperature and T_r is the reference or transition temperature.

The most important aspect during the simulations of cold spray particle impacting with the Lagrangian algorithm is the possible excessive distortion of elements near the contact surfaces, especially at a higher particle impact velocity. The main measures to cope with this problem in ABAQUS include ALE adaptive mesh controls, element distortion control and damage of material. As reported by Assadi et al. (Ref 4), although the ALE adaptive meshing can cope with the excessive element distortion at moderate and high particle impact velocities, frequent remeshing resulted in nonconserving energy variation of the output set, and in unphysical shape of the out-flowing jet of material at the interface. The preliminary results also showed this phenomenon. In addition, the large length ratio (nominally from 0 to 1) in element distortion control can also cause the unreasonable shape of the deformed particle. Therefore, the material damage model was also considered. The failure elements at the contact interface can be deleted when some failure conditions are encountered, such as the excessive deformation and high temperature. It seems that the materials are extruded from the interface to form the jet (of course, the true jet by just element deletion cannot be obtained), which may also corresponds to the shear instability. In addition, the element deletion using the damage model can also lead to important influence on the deformed particle shape and the output. These results will be given in the following section. The Johnson and Cook damage model (referred to as the ''Johnson-Cook dynamic failure model'' in ABAQUS) was used, which accounts for the effects of hydrostatic pressure, strain rate, and temperature (Ref 14). ABAQUS/Explicit also offers a more general implementation of the JC failure model as part of the family of damage initiation criteria, which is the recommended technique for modeling progressive damage and failure of materials. The JC dynamic failure model is based on the value of the equivalent plastic strain at element integration points, where failure is assumed to occur when the damage parameter exceeds 1. The damage parameter, ω, is defined as

$$\omega = \sum \left(\frac{\Delta \bar{\varepsilon}_p}{\bar{\varepsilon}_{pf}} \right) \quad \text{(Eq 3)}$$

where $\Delta\bar{\varepsilon}_p$ is an increment of the equivalent plastic strain, $\bar{\varepsilon}_{pf}$ is the strain at failure, and the summation is performed over all increments in the analysis. The strain at failure is assumed to be dependent on a nondimensional plastic strain rate, $\dot{\varepsilon}^*$; a dimensionless pressure-deviatoric stress ratio, p/q (where p is the pressure stress and q is the Mises stress); and the nondimensional temperature, T^*, defined

earlier in the JC plasticity model. The dependencies are assumed to be separable and are of the form:

$$\bar{\varepsilon}_{pf} = \left[d_1 + d_2 \exp\left(d_3 \frac{p}{q}\right)\right][1 + d_4 \ln(\dot{\varepsilon}^*)](1 + d_5 T^*) \quad \text{(Eq 4)}$$

where d_1-d_5 are failure parameters measured at or below the transition temperature, T_r. When this failure criterion is met, the deviatoric stress components are set to zero and remain zero for the rest of the analysis. Depending on the selected values, the pressure stress may also be set to zero for the rest of calculation (if this is the case, it must be specified element deletion and the element will be deleted) or it may be required to remain compressive for the rest of the calculation (if this is the case, it must be chosen not to use element deletion). By default, the elements that meet the failure criterion are deleted. It can be specified the fracture energy per unit area, G_f, to be dissipated during the damage process directly, which means defining damage evolution based on energy dissipated in ABAQUS. Instantaneous failure will occur if G_f is specified as 0. However, this choice is not recommended and should be used with care because it causes a sudden drop in the stress at the material point that can lead to dynamic instabilities. Therefore, the evolution in the damage was specified in exponential form in this study. Other detailed information can be found in the ABAQUS Analysis User's Manual (Ref 14).

Because of the excellent cold sprayablity of copper, it has been widely studied experimentally. In this study, Cu was also employed as the objective material based on its easily available material data (e.g., Ref 15) used in simulations as shown in Table 1. The mechanical and thermal material properties were assumed to be isotropic. It was also assumed that the initial temperatures of particle and substrate (T_o) are 25 °C. The initial velocity of particle (v_p) is dependent on the conditions to be study. Hereafter, it is fixed at a moderate value of 500 m/s because the simulations work well in most cases at a low impact velocity, e.g., 300 m/s. In addition, the total solution time is set as 60 ns.

3. Results and Discussion

According to our preliminary results by ABAQUS, some important setting factors involving in the simulations were investigated. It should be pointed out that the element output includes mainly the effective plastic strain (PEEQ), stress and temperature, which is element-averaged because the used elements are one-point integration. It should also be declared that just the studied setting factor is changed in the simulations to clarify its effect on the output, while the other settings are in the default state. Table 2 gives the default setting for the studied factors. It should also be pointed out that if element distortion control is not used, the program will finish abnormally with the excessively distorted elements under other default settings. Accordingly, the distortion control was used as a default setting. In addition, all the simulations are conducted without considering the oxide films and the possible adhesion between the particle and substrate, which will commonly cause the bounce of particle after simulations. This is not the issue to be discussed in this study.

Table 1 Properties of OFHC copper used in simulations (Ref 15)

Density, kg/m^3	8960
Thermal conductivity, W/(m °C)	386
Specific heat, J/(kg) (°C)	383
Melting point, °C	1083
Expansion coefficient, 1/°C	0.00005
Elastic modulus, GPa	124
Poisson's ratio	0.34
JC plasticity: A, MPa, B, MPa, n, C, m	90, 292, 0.31, 0.025, 1.09
JC damage: d1, d2, d3, d4, d5	0.54, 4.89, −3.03, 0.014, 1.12
Reference temperature, °C	25
Reference strain rate, 1/s	1

3.1 Effect of Solution Procedure

As reported by Assadi et al. (Ref 4) and Grujicic et al. (Ref 8), the impacting process was assumed to be an adiabatic process; i.e., the heat transfer is not considered based on a simple estimation. However, the recent study by Schmidt et al. (Ref 5) indicated that the heat conduction should be considered in most cases. There are two analysis procedures to deal with short dynamic processes in ABAQUS. One is the dynamic explicit procedure (Dynamic-Explicit), which can be used to perform an adiabatic stress analysis if inelastic dissipation is expected to generate heat in the material, as used by Assadi et al. (Ref 4) and Grujicic et al. (Ref 8). Another one is a fully coupled thermal-stress analysis procedure (Dynamic-Temp-Disp-Explicit), which is performed when the mechanical and thermal solutions affect each other strongly, and therefore, must be obtained simultaneously, as adopted by Schmidt et al. (Ref 5).

Table 2 Default settings of the studied factors in the simulations (Ref 14)

Setting factor	Default	Variation
Solution procedure	Dynamic-Temp-Disp-Explicit	Dynamic-Explicit
Hourglass control	Stiffness	Enhanced, Relax Stiffness, Viscous, combined with stiffness-viscous weight factor: 0.5 and 0.9
Element distortion Control	Length ratio: 0.1	Length ratio: 0.4, 0.8
ALE adaptive meshing	NO (exclusively without distortion control)	YES, Frequency: 100, 50, 10, 5, 1; Remeshing sweeps per increment: 1, 5
Interface friction	NO	Coefficient of friction (COF): 0.2, 0.4
Material damage	NO	YES
Meshing Size	1/50d_p	1/20d_p, 1/100d_p

Figure 2 shows the simulation results obtained by these two solution procedures. Both the procedures finished normally in 60 ns. It is seen that although they yield the extremely similar shapes of the deformed particle and substrate, much higher temperature and temperature localization at the interface are clearly observed using the Dynamic-Explicit procedure (Fig. 2b). With the Dynamic-Temp-Disp-Explicit procedure, obvious heat conduction from the interface to inner particle and substrate is found (Fig. 2e). It is also noticed that a higher maximum PEEQ is obtained at the interface using the Dynamic-Explicit procedure than using the Dynamic-Temp-Disp-Explicit procedure. The large differences in the PEEQ and temperature during the impacting process can also be clearly observed from Fig. 2(c) and (f). Therefore, the present results clarified that heat conduction should be considered

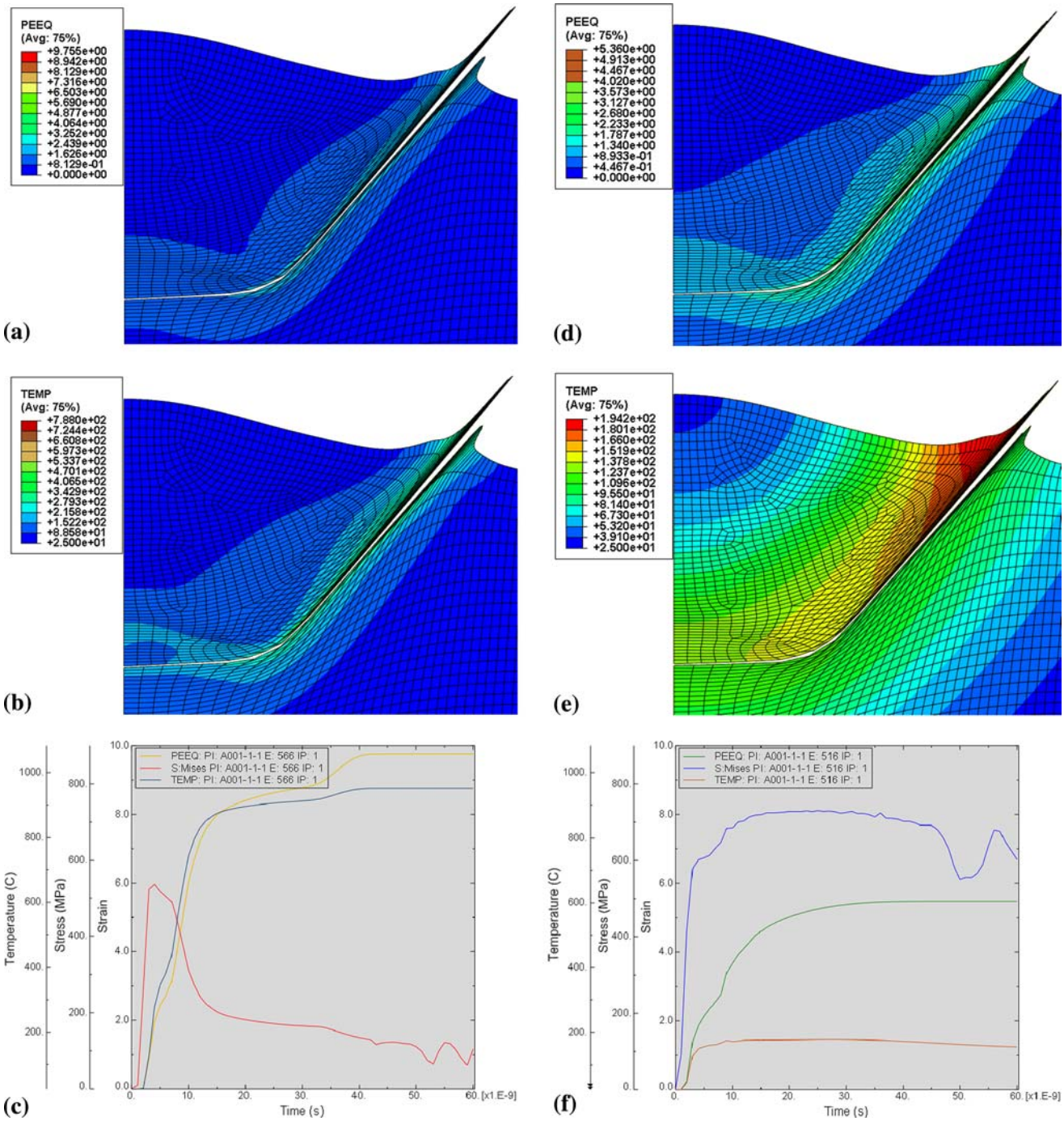

Fig. 2 Simulated contours of PEEQ (a, d) and temperature (b, e) and temporal evolutions of temperature, stress and strain (c, f) using the Dynamic-Explicit (a-c) and Dynamic-Temp-Disp-Explicit (d-f) procedures

in the simulations of cold spray particles impacts. As documented in the ABAQUS manual (Ref 14), although the Dynamic-Explicit procedure is computationally efficient for the analysis of large models with relatively short response times and for the analysis of extremely discontinuous events, fully coupled thermal-stress analysis is needed when the stress analysis is dependent on the temperature distribution and the temperature distribution depends on the stress solution. For such cases, the thermal and mechanical solutions must be obtained simultaneously rather than sequentially.

3.2 Effect of Hourglass Control

It is known that hourglass control is a very useful method to minimize the problems involved in the reduced-integration elements without introducing excessive constraints on the element's physical response. Several methods are available in ABAQUS for suppressing the hourglass modes, including the techniques based on Stiffness, Relax Stiffness, Enhanced, Viscous, and Combined Stiffness-Viscous. According to the preliminary simulations, the Stiffness, Enhanced, and Combined methods are important for modeling cold spray particles impacts. With the Stiffness technique, the program can finish normally as shown in Fig. 2. But for the other techniques, the program aborted due to the excessive distortion of elements causing the exaggerated temperature fields as shown in Fig. 3 (just three cases). The further study showed that those hourglass control techniques can work when combined with other settings, such as ALE adaptive meshing and material damage.

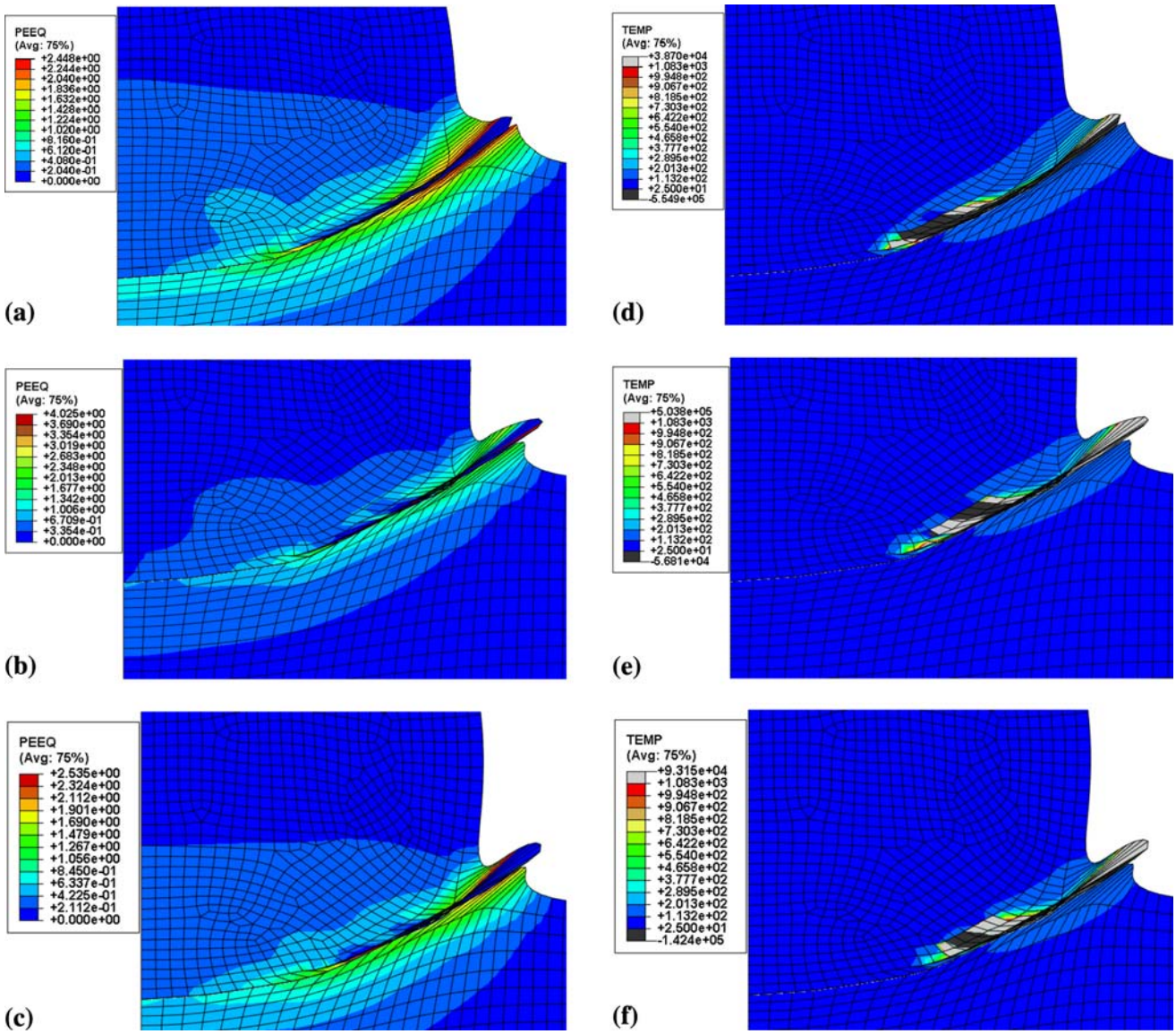

Fig. 3 Simulated contours of PEEQ (a-c) and temperature (d-f) with the techniques of Enhanced (a, d, fails at around 13 ns), Combined of a stiffness-viscous weight ratio of 0.5 (b, e, fails at around 11 ns) and combined of a stiffness-viscous weight ratio of 0.9 (c, f, fails at around 10 ns)

3.3 Effect of Element Distortion Control

Without element distortion control, analyses may fail prematurely when the mesh is coarse relative to strain gradients and the amount of compression. ABAQUS/Explicit offers distortion control to prevent solid elements from inverting or distorting excessively for these cases. Constraints are enforced by using a penalty approach, and one can control the associated distortion length ratio. Distortion control cannot be used when the elements are included in an adaptive mesh domain (mutually exclusive in ABAQUS) (Ref 14). In this study, the analysis failed prematurely at around 17 ns without element distortion control. Hence a distortion length ratio of 0.1 was used as the default setting. Figure 4

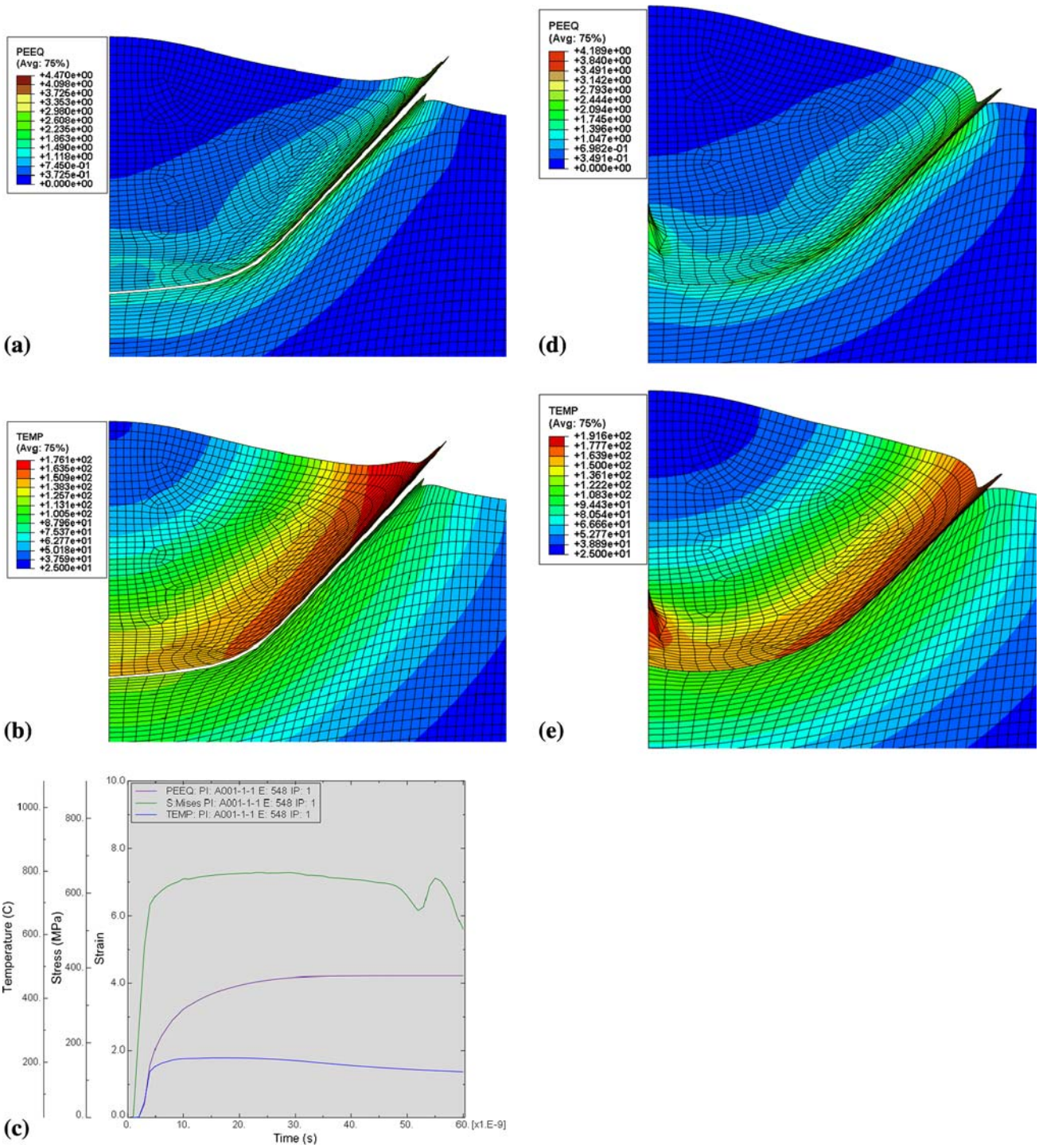

Fig. 4 Simulated contours of PEEQ (a, d) and temperature (b, e) and temporal evolutions of temperature, stress and strain (c) with the distortion length ratios of 0.4 (a-c) and 0.8 (d, e, fail at about 40 ns)

gives the results with higher distortion length ratios. It is found that the maximum PEEQ and temperature values obtained with the length ratio of 0.4 are lowered compared to those obtained with the length ratio of 0.1 (Fig. 2d, e and f). A little change in jet shapes is also observed. However, for the length ratio of 0.8 (Fig. 4d and e), the program failed at about 40 ns due to the much constraint to element deformation. As documented in the ABAQUS manual (Ref 14), care must be used in interpreting results since the distortion control constraints may inhibit legitimate deformation modes and lock up the mesh. In addition, distortion control cannot prevent elements from being distorted due to temporal instabilities, hourglass instabilities, or physically unrealistic deformation. Therefore, the distortion length ratio is, if required, usually of a small value; e.g., 0.1.

3.4 Effect of ALE Adaptive Meshing

The ALE adaptive meshing technique in ABAQUS combines the features of pure Lagrangian analysis and pure Eulerian analysis. It is a tool that makes it possible to maintain a high-quality mesh throughout an analysis, even when large deformation or loss of material occurs, by allowing the mesh to move independently of the material (Ref 14). However, in some extreme cases, it does not work well. Based on the preliminary results, just frequency and remeshing sweeps per increment were considered with other settings as default in this study. Figure 5 shows the simulation results obtained with different combinations of frequency and remeshing sweeps per increment, with which the program finished normally. It is seen that with decreasing the frequency, i.e., increasing the remeshing times in given increments, the maximum PEEQ and temperature are decreased and the jet shape appears more smooth, in other words, more unrealistic deformation of the periphery (Fig. 5a, b, d, and e) compared to the result without ALE adaptive meshing (Fig. 2). When increasing the remeshing sweeps per increment (Fig. 5c and f); i.e., more remeshing is performed per increment, the maximum PEEQ and temperature and contours seem to be changed a little as compared to Fig. 5(b) and (e). However, these two factors are interactional, because in other combinations of frequency and remeshing sweeps per increment the program aborted due to excessive distortion of some element, such as 100-1 (frequency-remeshing sweeps per increment), 5-1, 100-5, and 10-1 (fail at about 12 ns). In these cases, ALE adaptive meshing may be combined with other techniques, such as material damage, to make it work. Nevertheless, ALE adaptive meshing is not strongly recommended to use in modeling cold spray particles impacts owing to the unrealistic jet as indicated by Assadi et al. (Ref 4).

3.5 Effect of Interface Friction

In the previous study on particle/substrate interaction (Ref 4-10), no friction between the particle and substrate was considered. Therefore, friction was included for the first time in this study by using the available friction models in ABAQUS. There are several friction models in ABAQUS, such as the basic Coulomb friction model, shear stress versus elastic slip while sticking, exponential decay friction model (Ref 14). The simple Coulomb friction model was used in this study. Figure 6 shows the simulation results obtained with the constant COFs of 0.2 and 0.4. It is found that the maximum PEEQ and temperature at the interface are lowered when friction is considered compared to the frictionless state (Fig. 2). The jet formation is also limited due to the friction shear stress. However, the value of COF has a little effect on the resultant output in the range from 0.2 to 0.4 as shown in Fig. 6. In addition, it is clearly observed from that friction takes a small role in increasing the internal energy during the particle impacting process compared to the plastic dissipation. Therefore, a small COF is appropriate in modeling cold spray particles impacts. It should be point out that with the basic Coulomb friction model, which does not specify a limiting shear stress, the interface shear stress may be overestimated in the case with extremely high contact pressure.

As mentioned above, one can make the program with the meshing size of $1/100d_p$ be conducted without abortion by the combination of other solution techniques, such as ALE adaptive meshing and material damage (Fig. 7c). Through the preliminary study, the program can finish normally using the ALE adaptive meshing with the frequency-remeshing sweeps per increment of 1-5 and the enhanced hourglass control as shown in Fig. 8.

3.6 Effect of Material Damage

Although the abovementioned calculation techniques can be performed successfully to yield comparable output, sometimes they do not work well; e.g., when the meshing size is relatively fine which can result in more precise data. Therefore, the material failure model was examined for the first time in this study according to the suggestion documented in the ABAQUS manual. Here the slave surface in the interaction definition must be node region to be possibly eroded; while the Status variable must be selected in the field output requests. Figure 7 shows the typical simulation results obtained with the JC failure model. It is found that the elements of large deformation in the particle at the interface have been deleted from the calculation. Compared to the deformed shape without material damage (Fig. 2), the obtained particle shape with material damage seems more reasonable. It is expected to obtain a better shape of the deformed particle with a finer meshing size. However, when the meshing size is $1/100d_p$, the result (Fig. 7c) is not satisfactory owing to the unrealistic deformation of substrate elements at the interface, which cannot be set with material damage as the master surface in a 2D model (Ref 14). As a result, the 3D modeling may be very interesting in modeling the failure of both particle and substrate, where the erosion contact is permitted. The unrealistic deformation of substrate elements at the interface can be avoided with the 3D model, which has been examined and will present in another contribution.

3.7 Effect of Meshing Size

As has been recognized by Assadi et al. (Ref 4) using ABAQUS/Explicit and in our previous study (Ref 6, 9) using the LS-DYNA code which is also a popular explicit finite element method, the meshing density takes an important role in the computation and influences significantly the resultant output. However, Assadi et al. (Ref 4) did not explore this effect and present the effective measures to cope with it. Therefore, this research will give some validation and explanation on the effect of the relative meshing size. Figure 9 shows the simulation results obtained for the meshing sizes of $1/20d_p$ and $1/100d_p$. But the program failed prematurely at about 4 ns due to the excessive element distortion (Fig. 9d and e). In comparison with the result obtained for the meshing size of $1/50d_p$ (Fig. 2), the maximum PEEQ and temperature decrease for the meshing size of $1/20d_p$ (Fig. 9a, b and c). It is understandable taking into account the fact that the output is element-averaged and the used elements are one-point integration. From this point, it is expected that

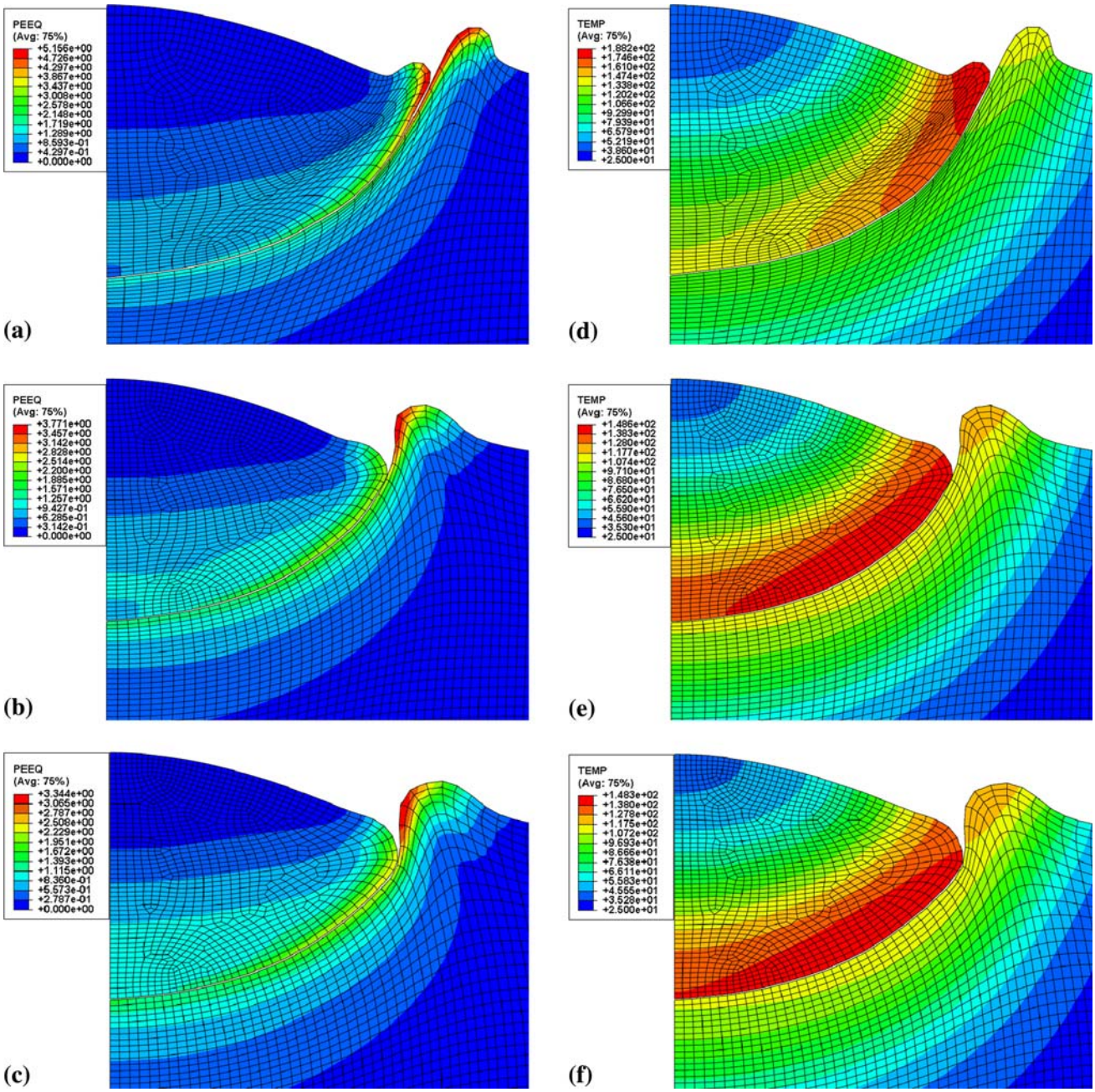

Fig. 5 Simulated contours of PEEQ (a-c) and temperature (d-f) with different ALE adaptive mesh combinations of frequency and remeshing sweeps per increment: (a, d) frequency-remeshing sweeps per increment 50-1, (b, e) 1-1, and (c, f) 1-5

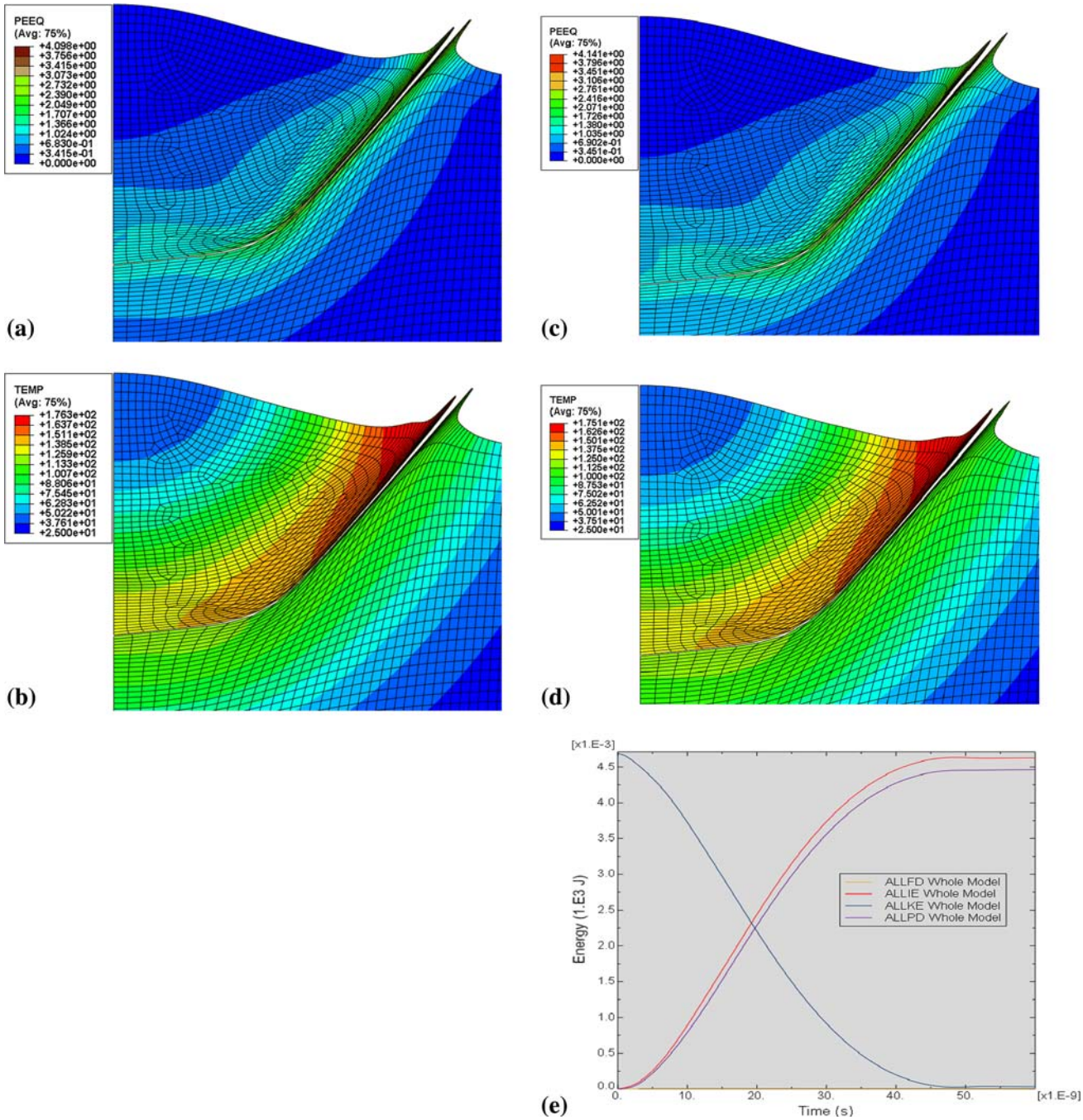

Fig. 6 Simulated contours of PEEQ (a, c) and temperature (b, d) and temporal evolutions of energies (e) with the constant contact surface COFs of 0.2 (a, b) and 0.4 (c-e). Note that ALLFD: friction dissipation, ALLPD: plastic dissipation, ALLIE: internal energy, ALLKE: kinetic energy

the finer meshing, the more approaching to the realistic data.

Based on the finding by Assadi et al. (Ref 4), the onset velocities of excessive element distortion under different meshing sizes are given in Fig. 10. For comparison, the simulation results on Cu obtained by LS-DYNA are also plotted in Fig. 10. If this onset velocity is taken as the so-called critical velocity by Assadi et al. (Ref 4), it is seen that the critical velocity decreases with decreasing the meshing size for the same material. It is also found that the instability velocities for different materials tend to be 300-400 m/s, even for the high strength In718 alloy, which is much lower than the reported critical velocities (Ref 5, 8). According to

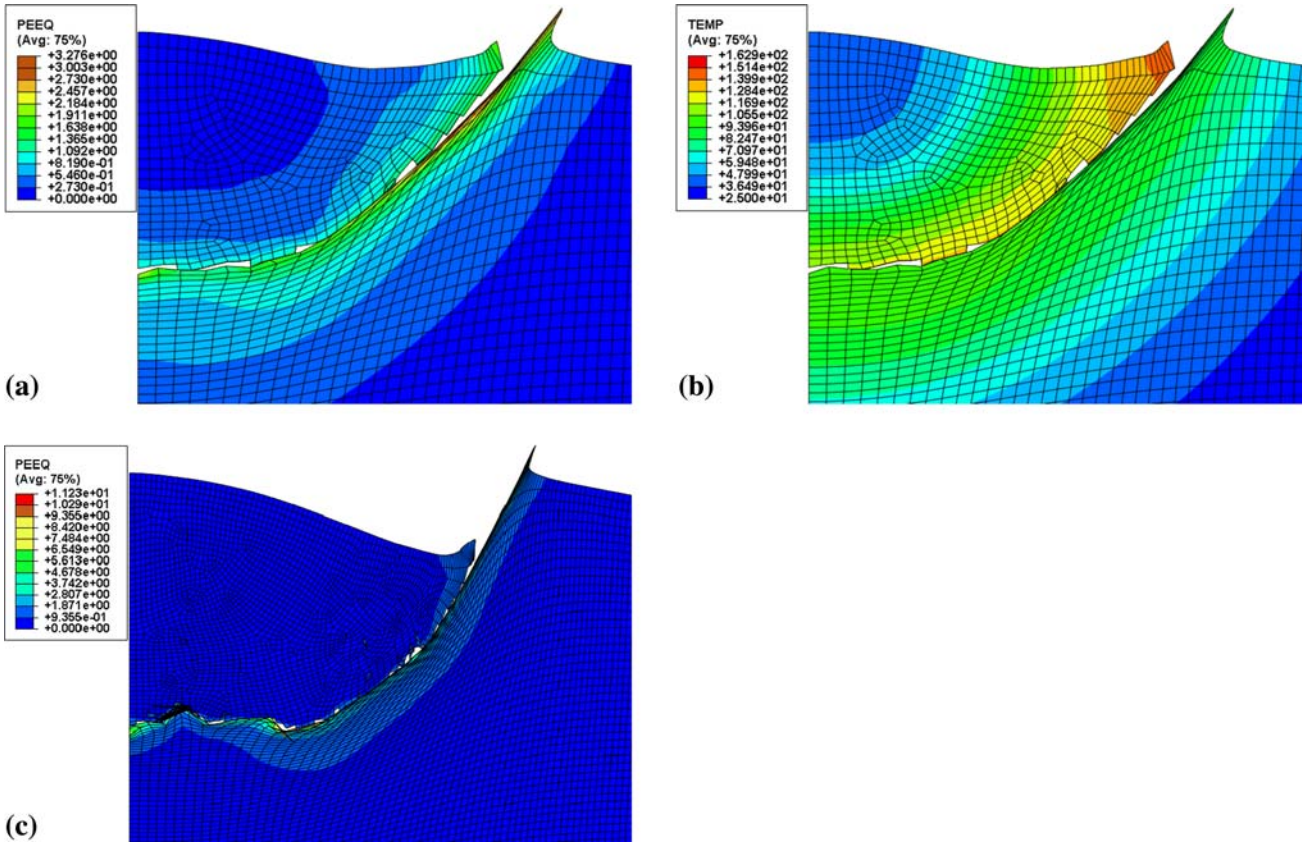

Fig. 7 Simulated contours of PEEQ (a, c) and temperature (b) with the material damage model for the meshing sizes of $1/50d_p$ (a, b) and $1/100d_p$ (c)

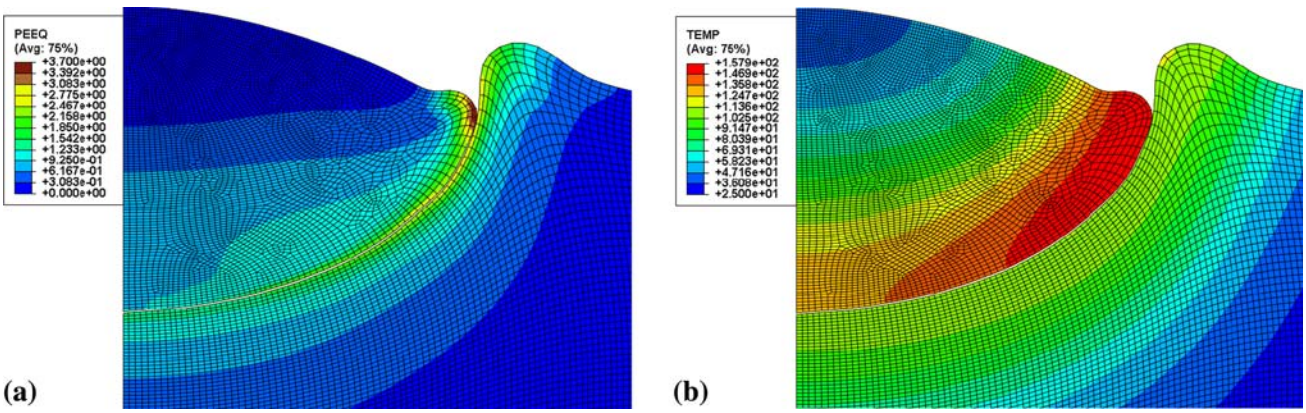

Fig. 8 Simulated contours of PEEQ (a) and temperature (b) for the meshing size of $1/100d_p$ using the ALE adaptive meshing with the frequency-remeshing sweeps per increment of 1-5 and the enhanced hourglass control

the previous study (Ref 6), a critical velocity of about 300 m/s for Cu of low oxygen content was found. Schmidt et al. (Ref 5) also reported an adhesion velocity of about 250 m/s for 20 mm Cu spherical projectile. Therefore, the dominant effect of particle oxidation state was proposed in the previous study (Ref 6) explaining well the up-to-date findings by different research groups. Kang et al. (Ref 12) later reported the similar oxidation dependency of aluminum powders and proved our model. However, much work is necessarily required to reveal the realistic adiabatic shear instability by numerical and experimental methods.

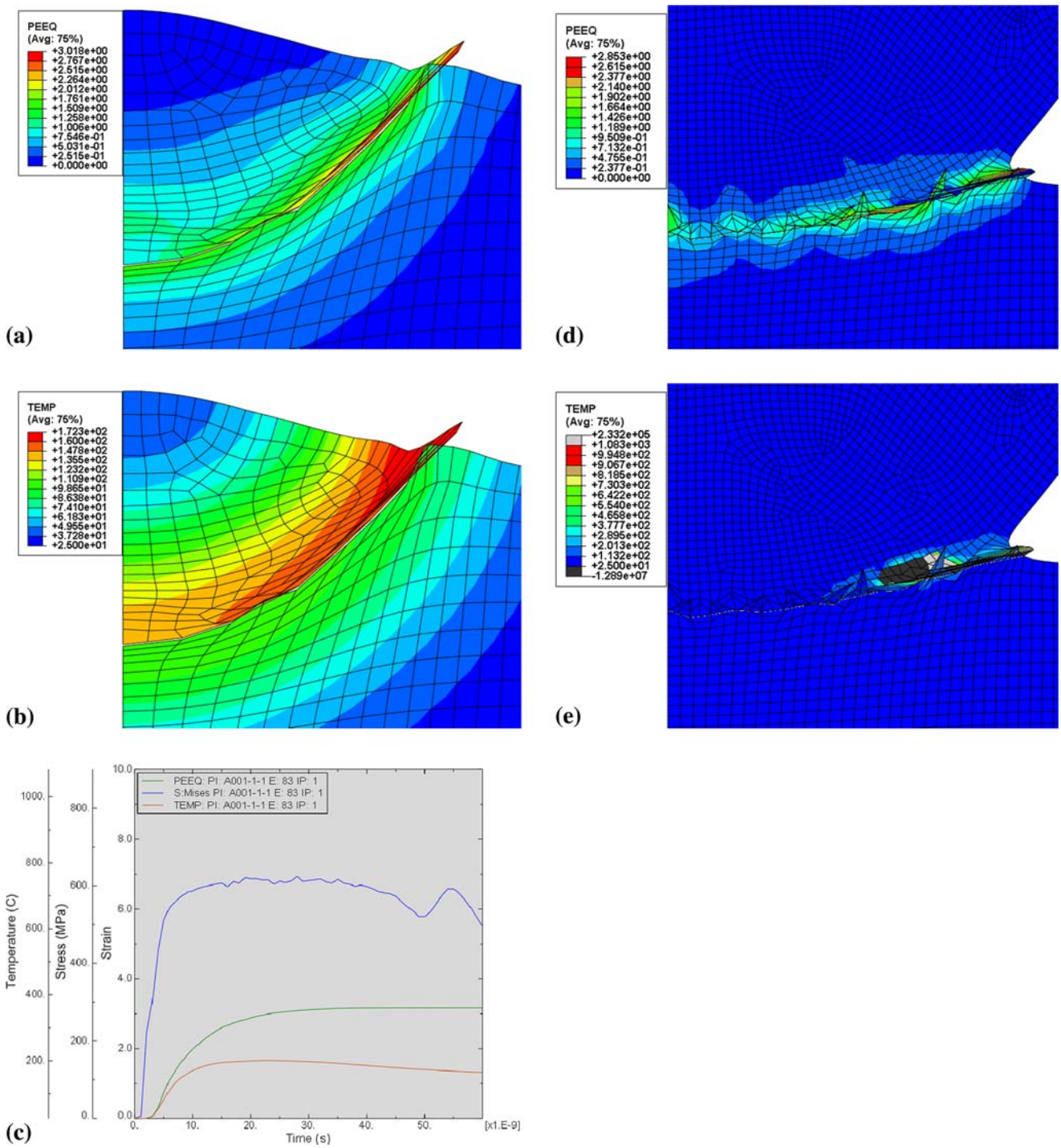

Fig. 9 Simulated contours of PEEQ (a, d) and temperature (b, e) and temporal evolutions of temperature, stress and strain (c) with the meshing sizes of $1/20d_p$ (a-c) and $1/100d_p$ (d, e, fail at about 4 ns)

4. Concluding Remarks

Through the systematic investigation of the effects of the simulation settings on the output in modeling the impacting behavior of cold spray particles, the feasibility and capability of numerical simulation of particle impacting by the ABAQUS/Explicit program were evaluated. The results showed that the satisfactory output could be obtained with the appropriate settings, but careful regulation of the setting factors is necessary. No mater which solution technique is used, the main objective is to model the physical processes occurred in cold spray particles impacts, such as metal jetting, adiabatic shear instability, oxide film effect, and final adhesion between

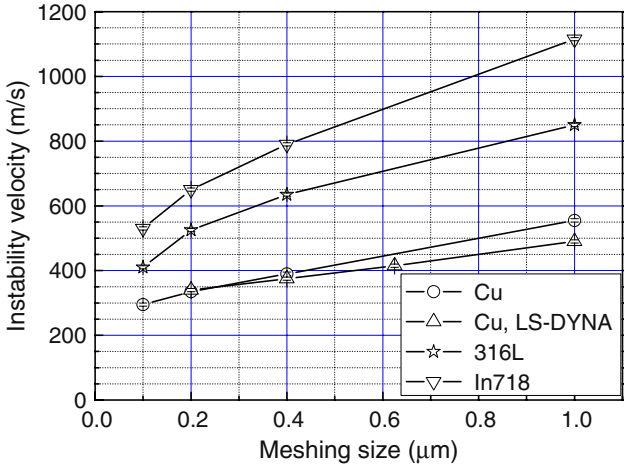

Fig. 10 Effect of meshing size on the onset velocity of element instability for different materials

the particle and substrate. The future work on the effect of particle size and the 3D modeling may be necessary to investigate more complex impacting conditions, such as the erosion of the particle and substrate, off-normal impact, and multi-particle impact.

Acknowledgments

This work was partially supported by the NPU Talent Development Foundation, the Scientific and Technological Innovation Foundation for Youth NPU Teachers, and the Ao-Xiang Star Project.

References

1. A. Papyrin, Cold Spray Technology, *Adv. Mater. Proc.*, 2001, **159**(9), p 49-51
2. T. Stoltenhoff, H. Kreye, and H.J. Richter, An Analysis of the Cold Spray Process and its Coatings, *J. Therm. Spray Technol.*, 2002, **11**, p 542-550
3. R.C. Dykhuizen, M.F. Smith, D.L. Gilmore, R.A. Neiser, X. Jiang, and S. Sampath, Impact of High Velocity Cold Spray Particles, *J. Therm. Spray Technol.*, 1999, **8**, p 559-564
4. H. Assadi, F. Gärtner, T. Stoltenhoff, and H. Kreye, Bonding Mechanism in Cold Gas Spraying, *Acta Mater.*, 2003, **51**(15), p 4379-4394
5. T. Schmidt, F. Gärtner, H. Assadi, and H. Kreye, Development of a Generalized Parameter Window for Cold Spray Deposition, *Acta Mater.*, 2006, **54**, p 729-742
6. C.J. Li, W.Y. Li, and H.L. Liao, Examination of the Critical Velocity for Deposition of Particles in Cold Spraying, *J. Therm. Spray. Technol.*, 2006, **15**(2), p 212-222
7. M. Grujicic, J.R. Saylor, D.E. Beasley, W.S. DeRosset, and D. Helfritch, Computational Analysis of the Interfacial Bonding between Feed-Powder Particles and the Substrate in the Cold-Gas Dynamic-Spray Process, *Appl. Surf. Sci.*, 2003, **219**, p 211-227
8. M. Grujicic, C.L. Zhao, W.S. DeRosset, and D. Helfritch, Adiabatic Shear Instability Based Mechanism for Particles/Substrate Bonding in the Cold-Gas Dynamic-Spray Process, *Mater. Design*, 2004, **25**, p 681-688
9. W.Y. Li, H.L. Liao, C.J. Li, G. Li, C. Coddet, and X.F. Wang, On High Velocity Impact of Micro-sized Metallic Particles in Cold Spraying, *Appl. Surf. Sci.*, 2006, **253**(5), p 2852-2862
10. W.Y. Li, H.L. Liao, C.J. Li, H.-S. Bang, and C. Coddet, Numerical Simulation of Deformation Behavior of Al Particles Impacting on Al Substrate and Effect of Surface Oxide Films on Interfacial Bonding in Cold Spraying, *Appl. Surf. Sci.*, 2007, **253**(11), p 5084-5091
11. W.Y. Li, C. Zhang, H.T. Wang, X.P. Guo, H.L. Liao, C.-J. Li, and C. Coddet, Significant Influences of Metal Reactivity and Oxide Film of Powder Particles on Coating Deposition Characteristics in Cold Spraying, *Appl. Surf. Sci.*, 2007, **253**(7), p 3557-3562
12. K. Kang, S. Yoon, Y. Ji, and C. Lee, Oxidation Dependency of Critical Velocity for Aluminum Feedstock Deposition in Kinetic Spraying Process, *Mater. Sci. Eng. A*, 2008, **486**, p 300-307
13. C.J. Li and W.Y. Li, Effect of Sprayed Powder Particle Size on the Oxidation Behaviour of MCrAlY Materials during HVOF Deposition, *Surf. Coat. Technol.*, 2003, **162**(1), p 31-41
14. *Abaqus Analysis User's Manual*, ABAQUS 6.7 HTML Documentation, Dassault Systèmes, 2007
15. G.R. Johnson and W.H. Cook, Fracture Characteristics of Three Metals Subjected to Various Strains, Strain Rates, Temperatures and Pressures, *Eng. Fract. Mech.*, 1985, **21**(1), p 31-48